Int. J. Adv. Eng. Pure Sci. 2026, 38(3): <468-479>
DOI: 10.7240/jeps.1954934

RESEARCH ARTICLE / ARAŞTIRMA

Geostatistical and Spatial Clustering Analysis for Wildfire Monitoring in Türkiye

Türkiye'de Orman Yangınlarının İzlenmesi için Jeoistatistiksel ve Mekansal Kümeleme Analizi

Mehmet Şamil GÜNEŞ [1],

[1] Yıldız Teknik Üniversitesi, Fen-Edebiyat Fakültesi, İstatistik Bölümü, İstanbul, Türkiye

Abstract

The wildfire situation has become increasingly dangerous to the eastern Mediterranean's forest lands and human life. Among these are wildfires in Türkiye that have had one of the largest impacts on the country in the region. A pipeline consisting of five steps was applied using an integrated methodology to analyze MODIS Collection 6.1 data for the fires occurring in Türkiye during the three years of 2018 through 2020. The results were used to understand where, when and how much energy burned by wildfires throughout Türkiye. Five methods made up this process. The first method used to evaluate this information is FRP weighted Kernel Density Estimation (KDE) which provides the locations of highest concentration of fire in each year. The second method is Global Spatial Autocorrelation (Morans I) which examines whether fire occurs near other fires. Local Hotspot Detection (Getis-Ord Gi*) is the third method which identifies hotspots within individual grid cells. Interannual Difference Maps were produced using the fourth method to compare differences in FRP values from each year. Finally, the fifth method, Density-Based Spatial Clustering Analysis (DBSCAN), identified clusters of fire based on their geographic location. The southern central Anatolian belt (37°-38°N) continued to be identified as the area of greatest fire intensity, characterized by a large amount of FRP weighted density, statistically significant local hotspot concentrations (HS≥95%) in the same area in 2019 and was also located at the centroid of the DBSCAN cluster in all years studied. In addition to identifying areas with increased FRP, national average FRP values increased by about 22%, from 19MW in 2018 to 23MW in 2020. Additionally, the decline of 64% (from .233 to .083) in Global Morans I indicates an increase in both the intensity and dispersal of fire occurrence globally. The number of DBSCAN clusters increased from three in 2019 to seven in 2020; two additional clusters emerged in the northeast part of Anatolia and in eastern Thrace. Based on these findings it appears that there may be an early indication of changes in the structure of wildfires in Türkiye due to warming conditions in the eastern Mediterranean.
Keywords: fire radiative power, spatial autocorrelation, KDE, DBSCAN clustering, hotspot analysis

Öz

Doğu Akdeniz'in ormanlık alanları ve insan yaşamı için orman yangınları durumu giderek daha tehlikeli hale gelmiştir. Bunlar arasında, bölgedeki en büyük etkilerden birine sahip olan Türkiye'deki orman yangınları da yer almaktadır. 2018-2020 yılları arasında Türkiye'de meydana gelen yangınlar için MODIS Collection 6.1 verilerini analiz etmek amacıyla entegre bir metodoloji kullanılarak beş adımdan oluşan bir süreç uygulandı. Sonuçlar, Türkiye genelinde orman yangınlarının nerede, ne zaman ve ne kadar enerji tükettiğini anlamak için kullanıldı. Bu süreç beş yöntemden oluşmaktadır. Bu bilgiyi değerlendirmek için kullanılan ilk yöntem, her yıl en yüksek yangın yoğunluğunun yerlerini sağlayan FRP ağırlıklı Çekirdek Yoğunluk Tahmini (KDE)'dir. İkinci yöntem, yangının diğer yangınların yakınında olup olmadığını inceleyen Küresel Mekansal Otomatik Korelasyon (Morans I)'dir. Üçüncü yöntem, bireysel ızgara hücreleri içindeki sıcak noktaları belirleyen Yerel Sıcak Nokta Tespiti (Getis-Ord Gi*)'dir. Dördüncü yöntem kullanılarak, her yıldaki FRP değerlerindeki farklılıkları karşılaştırmak için Yıllar Arası Fark Haritaları oluşturulmuştur. Son olarak, beşinci yöntem olan Yoğunluk Tabanlı Mekansal Kümeleme Analizi (DBSCAN), yangın kümelerini coğrafi konumlarına göre belirledi. Güney Orta Anadolu kuşağı (37°-38°N), yüksek FRP ağırlıklı yoğunluğu, 2019'da aynı alanda istatistiksel olarak anlamlı yerel sıcak nokta konsantrasyonları (HS≥95%) ile karakterize edilen ve incelenen tüm yıllarda DBSCAN kümesinin merkezinde yer alan en yüksek yangın yoğunluğuna sahip alan olarak belirlenmeye devam etti. Artan FRP'ye sahip alanların belirlenmesine ek olarak, ulusal ortalama FRP değerleri 2018'deki 19 MW'tan 2020'de 23 MW'a yaklaşık %22 arttı. Ayrıca, Küresel Morans I'deki %64'lük düşüş (0,233'ten 0,083'e), küresel olarak yangın oluşumunun hem yoğunluğunda hem de yayılımında bir artışa işaret etmektedir. DBSCAN kümelerinin sayısı 2019'da üçten 2020'de yediye yükseldi; Anadolu'nun kuzeydoğu kesiminde ve Doğu Trakya'da iki ek küme daha ortaya çıktı. Bu bulgulara dayanarak, Doğu Akdeniz'deki ısınma koşulları nedeniyle Türkiye'deki orman yangınlarının yapısında değişikliklere dair erken bir işaret olabileceği görülmektedir.
Anahtar Kelimeler: yangın radyatif gücü, mekansal otokorelasyon, KDE, DBSCAN kümeleme, sıcak nokta analizi

Corresponding Author: Mehmet Şamil Güneş, **Tel**: 0212 383 44 17, **E-mail**: msgunes@yildiz.edu.tr
Submitted: 19.05.2026, **Revised:** 17.07.2026, **Accepted:** 25.07.2026

I. INTRODUCTION

Wildfires represent one of the most damaging types of natural disasters impacting forest systems and their biological diversity, carbon stores and human livelihoods globally [1]. Fire frequency, seasonal duration and total burned area have all shown increases over the last forty years in numerous parts of the globe because of the combination of increased warming through human-induced climate change; increasing alterations to precipitation regimes and extensive modifications to both land-use/vegetation type [2]. Trends are even greater within the Mediterranean region than elsewhere, due to its identification as one of the main global hotspots for climate change impacts, with warmer mean temperature and lessening summer rainfall and longer more extreme dry periods [3]. Therefore, fire weather danger across the Mediterranean region is projected to intensify substantially under mid and high-emission climate scenarios, with the frequency of extreme fire weather days expected to double by the end of the twenty-first century [4].

Türkiye situated at the eastern margin of the Mediterranean fire-climate system, is among the most fire-prone countries in the region. The country encompasses a wide range of bioclimatic zones from humid Black Sea forests to semi-arid Central Anatolian steps. Annual burned area in Türkiye exhibited a marked increase during the 2000s and 2010s, and the catastrophic 2021 fire season which fell immediately after the study period examined here resulted in the largest recorded burned area in the country's modern history, underscoring the urgency of improved spatial understanding of fire dynamics [5]. Despite this context, systematic quantitative analyses of the spatial organisation of fire intensity across Türkiye, and its interannual variability, remain comparatively scarce in the peer-reviewed literature.

Satellite remote sensing has become the primary observational basis for large-scale fire monitoring, owing to its synoptic spatial coverage, temporal consistency, and independence from ground-based reporting networks [6]. Among the available satellite-derived fire products, fire radiative power (FRP) is particularly valuable as a physically based measure of instantaneous fire intensity that is directly proportional to the rate of fuel consumption and biomass combustion [7].

The Moderate Resolution Imaging Spectroradiometer (MODIS), aboard the NASA Terra and Aqua platforms, provides near-daily global active fire detection at 1 km spatial resolution through the MCD14ML product [6], and FRP observations derived from this dataset have been widely applied in fire emission estimation, energy release quantification, and landscape-scale fire ecology [8]. The time span analyzed in this research from 2018 to 2020 included extreme and unusual weather conditions for fire (as was seen with the particularly severe 2020 fire season), which had been produced as a result of an unusual rise in temperature during the summer months of the Eastern Mediterranean. Therefore, it provides a good basis to compare fire years on an annual level.

Satellite-detected fire activity can be analyzed through quantitative spatial analytical techniques that allow researchers to characterize both spatial patterns and dynamic characteristics of fires. Furthermore, these methods enable the use of kernel density estimates (KDE) to create fire surface maps that provide a visual representation of the spatial gradient in fire intensity at locations not visible when viewing point map data [9]. Global spatial autocorrelation statistics, most notably Moran's *I*, quantify the degree to which high-intensity fire pixels cluster spatially, providing an index of fire regime organisation that is directly interpretable in ecological terms [10, 11]. Local hotspot statistics such as the Getis-Ord *Gi** further decompose global autocorrelation into spatially explicit clusters of statistically elevated or suppressed values [12]. Finally, density-based clustering algorithms such as DBSCAN provide parameter-free delineation of discrete fire clusters without requiring prior specification of cluster number [13]. These methods have been applied productively in fire research across Europe and North America [14], yet their integrated application to Turkish fire data using MODIS FRP observations has not previously been reported.

Present study applies a five-step integrated spatial analysis pipeline to MODIS Collection 6.1 active fire observations for Türkiye over three consecutive fire seasons (2018–2020). The specific objectives of the study are: (i) to characterise the spatio-temporal distribution of FRP-weighted fire density using kernel density estimation and to map interannual density changes; (ii) to quantify global spatial autocorrelation in gridded mean FRP using Moran's *I* and to assess its statistical significance by permutation testing; (iii) to identify statistically significant local fire intensity hotspots using the Getis-Ord *Gi** statistic at multiple confidence thresholds; (iv) to detect and map interannual changes in cell-level mean FRP through difference mapping; and (v) to delineate discrete spatial fire clusters using DBSCAN and to characterise their size, location, and temporal evolution. The objective is for these findings to provide a body of evidence to inform three key areas of use within both the eastern Mediterranean (broadly) and Türkiye specifically: spatially explicit fire risk assessments, adaptive forest management plans, and early warning system designs.

II. STUDY AREA AND DATASET

2.1 Study Area

The focus of this research is the territory of Türkiye, which is located at the intersection of Southeastern Europe and Southwestern Asia. It has an approximate latitude of 36°-42° and a longitude of 26°-45°. Türkiye is approximately 783,562 square kilometers in size and contains some of the world's greatest diversity in terms of ecological zones. These include the Mediterranean, Aegean, Black Sea, Central Anatolia, and Eastern Anatolia. Each zone has its own unique vegetation cover, climatic regimes, and wildfire behavior characteristics. [15].

Türkiye's geographical structure, consisting of coastal plains and several mountainous areas with peaks greater than 3000 meters above sea level, also produces significant longitudinal variations in temperature, precipitation, and fuel moisture. Together, these variables create variability in the timing, duration, frequency, and location of wildfires. [16].

Figure 1. Spatial distribution of forest cover across Türkiye in 2020

Türkiye is one of the most fire-prone countries in the eastern Mediterranean basin. This region is designated a global climate change hotspot. Climate change will cause increases in surface temperatures and decreases in precipitation, leading to prolonged dry spells, increased fire weather, and longer fire seasons. [6].

For this research, MODIS data were used. Data consisted of fire detection products developed by FIRMS (NASA's Fire Information for Resource Management System) using MODIS Collection 6.1 Active Fires Product (MCD14ML). [16]. Data were retrieved over three consecutive years (January 2018 – December 2020), and all data were geographically filtered to be within the boundaries of Türkiye (EPSG:4326).

III. METHODS

This research's analytic methodology is based on an ordered series of five spatial-analysis techniques that have been performed using data from MODIS Active Fires (for the years 2018, 2019 & 2020). Each spatial analysis technique has been performed using Python version 3.12; scipy, geopandas, libpysal, esda, scikit-learn, and matplotlib are used as the required Python libraries.

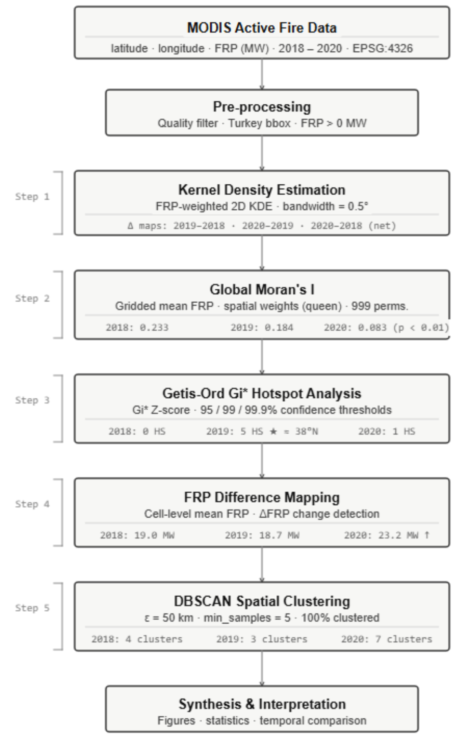

Figure 2. Workflow of study

As shown in the workflow (Figure 2), each step of the process begins with a "density" measure, then continues with "spatial-autocorrelation", followed by "hotspot-delineation", next "change-detection", and finally "unsupervised-spatial-clustering".

3.1 Data Pre-processing and Spatial Aggregation

Before being analyzed with these methods, MODIS MCD14ML point measurements had undergone a quality-control process. Those records containing fire radiative power (FRP) values less than/equal to 0 MW, or those which were identified as having confidence ratings lower than their designated threshold value, were deleted to limit the influence of commission errors caused by cloud edges, solar reflection artifacts, and long-term industrial heating sources. Those remaining records were spatially limited to the Turkish national boundary using the Global Administrative Area database.

No additional land-cover masking was applied prior to the analyses. Consequently, all MODIS Collection 6.1 active fire detections located within the national boundaries of Türkiye and satisfying the predefined quality-control criteria were retained regardless of the underlying land-cover type. The objective of this study was to characterize the national-scale spatial organization and temporal evolution of active fire occurrence rather than to distinguish among specific fire types. Therefore, both forest fires and other vegetation-related active fire detections (including agricultural burning where detected by MODIS) were included in the analyses.Before grid-based analyses (i.e., Moran's I and Getis-Ord Gi*), the point observations were spatially aggregated into a regular latitude-longitude grid having dimensions of 0.5° x 0.5°. This aggregation produced average FRP values at the grid-cell level. A 0.5° spatial resolution was chosen to find an appropriate compromise between the amount of detail provided by the spatial resolution of the data and the need to provide enough fire occurrences per grid cell to produce reliable autocorrelation statistics [17].

3.2 Kernel Density Estimation

Spatial fire density estimates were obtained from an application of a two dimensional Gaussian Kernel Density Estimator (KDE), using the coordinates of active fire detections as points, and weights based upon the corresponding Fire Radiative Power (FRP). FRP weighting has been utilized to place a higher weight on fires of higher intensities; thus, producing a density surface that represents the intensity of energy released per unit area, and is not simply a function of detection rate [7]. A kernel bandwidth of 0.5° or about 50km at middle latitudes was used for this analysis, because it is representative of the size scale of fire management units in Türkiye. Normalized density surfaces were then produced on a regular grid of 0.5° spacing. Differences in temporal density changes were analyzed via difference maps computed as:

$$\Delta D(t_1, t_2) = D(t_2) - D(t_1) \ (1) \tag{1}$$

where D(t) denotes the normalised FRP-weighted KDE surface for year t. Three difference maps were produced: 2019−2018, 2020−2019, and 2020−2018 (net change). Positive values indicate an increase in fire density between periods, whereas negative values denote a decrease.

3.3 Global Spatial Autocorrelation -Moran's I

Global spatial autocorrelation in gridded mean FRP was quantified using Moran's *I* statistic [10], defined as:

$$I = (n / S_0) \cdot (\Sigma_i \Sigma_j w_{ij} z_i z_j) / (\Sigma_i z_i^2) \tag{2}$$

where n is the number of grid cells, z_i is the mean-centred FRP value at cell i, w_{ij} is the spatial weight between cells i and j, and S_0 is the sum of all spatial weights. A queen-contiguity weights matrix (order 1) was constructed using *libpysal*, with row-standardisation applied so that each row sums to unity [18]. Statistical significance was assessed by means of a permutation test with 999 random permutations. Values of *I* significantly greater than the expected value under spatial randomness indicate positive spatial autocorrelation (i.e., clustering of similar FRP values), while values significantly below the expectation indicate dispersion [19].

3.4 Local Hotspot Analysis

Statistically significant fire intensity hotspots were identified using the Getis-Ord Gi* local spatial statistic (Getis & Ord, 1992), computed as:

$$Gi^* = (\Sigma_j w_{ij} x_j - \bar{X} \Sigma_j w_{ij}) / (S \cdot \sqrt{[(n \Sigma_j w_{ij}^2 - (\Sigma_j w_{ij})^2) / (n - 1)]}) \tag{3}$$

where x_j is the mean FRP value at cell j, $\bar{X}$ and S are the global mean and standard deviation of FRP across all cells, and w_{ij} are row-standardised queen-contiguity weights as defined in Section 3.3. The resulting Gi* z-score for each grid cell measures the degree to which local FRP values deviate from global expectations. Grid cells were classified as statistically significant hotspots (HS) or cold spots (CS) at three confidence levels: 95% ($|Z| > 1.96$), 99% ($|Z| > 2.576$), and 99.9% ($|Z| > 3.291$), following established conventions in spatial epidemiology and fire ecology [20]. Cells failing to meet the 95% threshold were designated as not significant.

3.5 FRP Difference Mapping and Change Detection

To determine how fire radiative power varied from one year to the next on a grid cell by grid cell basis, mean FRP surfaces were calculated for each year using the same 0.5° resolution and then used to create paired difference maps (e.g., 2019 vs. 2018; 2020 vs. 2019; and 2020 vs. 2018). Then, for all three comparisons, grid cells were categorized as either increased (where $\Delta FRP > 0$), decreased (where $\Delta FRP < 0$), or unchanged (where $\Delta FRP = 0$) and counts of cells within each category were recorded. This approach, analogous to post-classification change detection in land-cover analysis [21], enables the identification of spatial shifts in fire intensity and the delineation of areas with persistent or emerging high-FRP conditions. The net change surface (2020−2018) was interpreted as an indicator of multi-year trends in fire radiative power independent of year-to-year variability [18].

3.6 Density-Based Spatial Clustering - DBSCAN

Unsupervised spatial clustering of individual fire detections was performed using the Density-Based Spatial Clustering of Applications with Noise (DBSCAN) algorithm [13]. DBSCAN identifies clusters as high-density regions in feature space separated by areas of lower density and requires no prior specification of the number of clusters. The algorithm is governed by two parameters: the neighbourhood radius ε and the minimum number of points *MinPts* required to form a core point. Points that do not satisfy these criteria are classified as noise.

Fire detection coordinates (longitude, latitude) were converted to radians and DBSCAN was applied using the Haversine distance metric to account for the spherical geometry of the Earth [22]. The DBSCAN parameters were selected using a combination of data-driven analysis and methodological recommendations from the literature. First, the optimal neighborhood radius (ε) was determined by constructing a k-nearest-neighbor (k-NN) distance plot using the fifth nearest neighbor for each fire detection. The sorted k-NN distances exhibited a distinct elbow at approximately 50 km, indicating the transition between dense spatial clusters and noise. Consequently, ε was fixed at 50 km to capture the characteristic spatial extent of wildfire clusters while avoiding excessive cluster merging. The neighbourhood radius was set to ε = 50 km, consistent with the spatial extent of significant wildfire events in the Mediterranean region [14], and the minimum cluster size was fixed at *MinPts* = 5 detections. These parameters were selected through visual inspection of k-nearest-neighbour distance plots to identify the elbow point characteristic of the appropriate ε value [23]. For each cluster, the geographic centroid was computed, and the dominant cluster was defined as the cluster with the highest point count. This value provides a balance between detecting meaningful wildfire clusters and avoiding the identification of small groups of observations generated by random spatial variability. The selected parameter combination (ε = 50 km, MinPts = 5) produced spatial clusters that were geographically coherent and consistent with the wildfire distribution observed in the kernel density and hotspot analyses.

All analyses were conducted in Python 3.12. Spatial data analyses were used with geopandas 1.1 and pyproj 3.7 (Jordahl et al., 2021). Spatial weights matrices and global autocorrelation statistics were computed using libpysal 4.14 and ESDA 2.9 [24,31]. Kernel density estimation was implemented via scipy.stats.gaussian_kde [25]. The DBSCAN algorithm was applied using scikit-learn 1.5 [26]. Cartographic visualisations were produced with matplotlib 3.10 [27].

IV. RESULTS

The results are presented in five subsections corresponding to the sequential analytical steps described in Section 3. For each step, spatial patterns are characterised across the three study years (2018, 2019, 2020) and, where applicable, interannual trends are interpreted in the context of fire regime dynamics in Türkiye.

4.1 Spatio-temporal Kernel Density Estimation

The FRP-weighted kernel density surfaces reveal a persistent concentration of high-intensity fire activity in south-central and southwestern Türkiye across all three study years, with the highest normalised density values recorded in the area around 37°–38°N, 35°–38°E (Figure 3). In 2018, the density surface exhibited the most spatially compact hotspot, with peak values localised near the Taurus Mountain foothills and the eastern Mediterranean coastal belt. The 2019 surface displayed a broadly similar spatial pattern but with a secondary concentration emerging in the Aegean interior, accompanied by a measurable reduction in peak density relative to 2018 in the south-central zone. The difference map for 2019 - 2018 (Figure 3, bottom-left panel) indicates an increase in FRP-weighted density across parts of the Aegean region (positive values, shown in red), concurrent with decreases in the eastern Mediterranean and central Anatolian zones (negative values, shown in blue).

KDE results suggest a geographically stable yet spatially evolving fire regime in Türkiye over the 2018–2020 period. The persistence of the south-central Anatolian fire belt as the dominant zone of high FRP-weighted density across all three years indicates that structural landscape and climatic factors including topographic exposure, fuel continuity, and the intensity of summer drought exert a consistent first-order control on fire intensity at the regional scale [16]. At the same time, the emergence of secondary density concentrations in the Aegean interior in 2019, and the marked intensification and partial eastward displacement of the density maximum in 2020, point to interannual variability driven by synoptic weather anomalies and antecedent fuel moisture conditions [4].
These spatial trends provide critical insights into where to allocate wildfire prevention, detection, and suppression efforts in a way that can be both adaptive and effective across the full range of fire-prone lands throughout Türkiye.

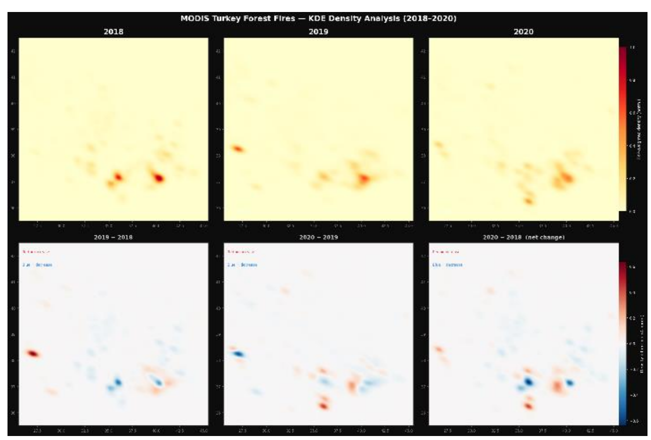

Figure 3. Weighted kernel density surfaces for 2018, 2019, and 2020 (top row), and interannual difference

maps (bottom row). Red tones indicate density increases; blue tones indicate decreases.

T The large-scale, progressive eastward trend in net change from 2020-2018 may indicate an accumulation of dryness in land cover due to longer-term declines in precipitation over multiple years, which is consistent with recent observed decreases in soil moisture and increases in drought severity across the eastern Mediterranean. The net change surface (2020-2018) (Figure 3, bottom-right panel) confirms a sustained increase in FRP density in the southwestern coastal zone and a partial eastward shift of the fire density maximum over the three-year period.

4.2 Global Spatial Autocorrelation - Moran's I

Global Moran's I statistics computed for gridded mean FRP indicate statistically significant positive spatial autocorrelation in all three study years, confirming that grid cells with high FRP values tend to be spatially adjacent to other high-FRP cells (Table 1; Figure 4).

The Moran scatter plots (Figure 4, top row) show that the majority of observations cluster in the high–high (HH) quadrant of the plot, indicative of spatially contiguous fire intensity hotspots, with a smaller proportion in the low–low (LL) quadrant representing areas of uniformly low fire activity.

Table 1. Global Moran's I statistics

Year	Moran's I	Z-score	p-value
2018	0.2332	8.702	0.001
2019	0.1842	6.974	0.001
2020	0.0832	3.205”	0.006

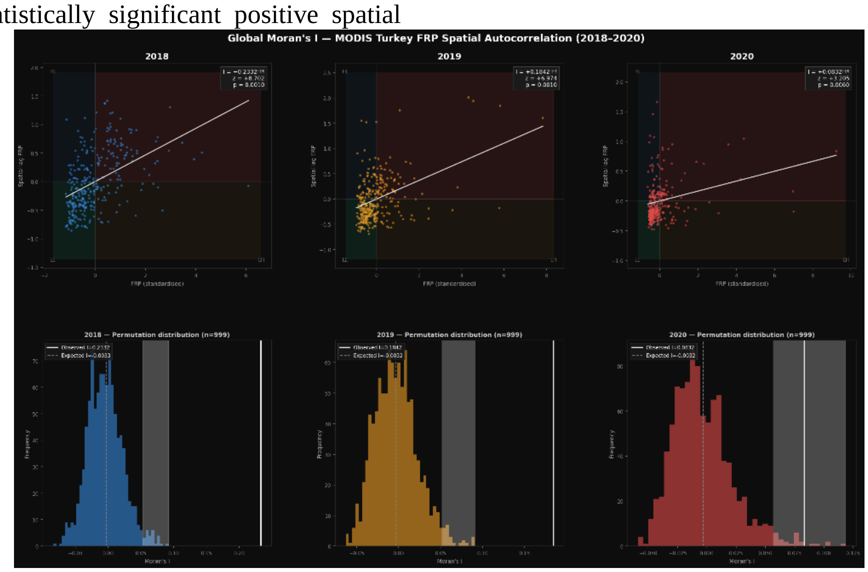

Figure 4. Global Moran's I Moran scatter plots (top row) and permutation reference distributions (bottom row) for 2018 (blue), 2019 (amber), and 2020 (red).

A statistically significant declining trend in Moran's I is evident across the study period: from I = 0.2332 (Z = +8.702, p = 0.001) in 2018 to I = 0.1842 (Z = +6.974, p = 0.001) in 2019, and further to I = 0.0832 (Z = +3.205, p = 0.006) in 2020. Although there is still evidence for spatial clustering in each year as measured by the statistical significance of the autocorrelation coefficient (I), the size of the autocorrelation coefficient decreased by about 64% from 2018 to 2020 indicating increasing spatial dispersion of Fire Radiative Power (FRP). The permutation reference distributions (See Figure 4: Bottom Row) also show that observed I values are at least at the 99th percentile of the null distribution in both 2018 and 2019 and at or greater than the 95th percentile in 2020.

4.3 Local Hotspot Analysis

There are statistically significant fire intensity hot-spots at varying confidence levels for each study year according to the Getis-Ord Gi* analysis (Figure 5).

Although the Global Autocorrelation of Fire Intensity was significantly positive during all study years (as determined by Moran's I) no grid cells were meeting the criteria for Hotspot Classification at the 95 % level of significance in 2018; hence, although local concentrations of high FRP values may have been sufficient to indicate some form of localised autocorrelation, they were insufficiently extreme relative to their immediate neighbours to be formally classified as hotspots at this resolution. There were also no Cold Spots identified for any study years.

Figure 5. Getis-Ord Gi* maps (top row) and hotspot classification maps (bottom row) for 2018, 2019, and 2020.

The notable spatial concentration of statistically significant hot-spots occurred during the year 2019; 5 grid-cells were classified as High Spatial Concentration >95%, primarily located in southern central Anatolia, approximately at latitude 36° – 38 ° N (Figure 5, middle panels). The spatial pattern of higher than average Gi* z-score in 2019 is coincident with the secondary concentration of fire densities identified using Kernel Density Estimation analysis (Section 4.1), which supports the conclusion that the fires occurring during 2019 were characterized by both high-intensity localized fire activity and by relatively small geographic areas. During 2020, only one grid cell attained High Spatial Concentration (HS > 95%) status, and it was located on the Eastern Mediterranean coastal zone, approximately at latitude 38°N. The decrease in the number of hot-spot classifications from 2019 to 2020 is consistent with the spatial dispersion of fire activity inferred from the decreasing Moran's I statistic.

4.4 Interannual Change in Fire Radiative Power

Mean cell-level FRP surfaces and their corresponding pair-wise difference maps show large changes in annual variation in fire intensity over the entire country of Türkiye (Table 2; Figure 6). Over the course of this three-year study, the total amount of fire radiative power per square kilometres for the whole of Türkiye (mean FRP) was: 19.0 MW in 2018 (a low); it dropped slightly to 18.7 MW in 2019, but then jumped to 23.2 MW in 2020, an increase of about 22% from 2018. These elevated levels of mean FRP in 2020 are supported by reports of extreme fire weather throughout much of the Eastern Mediterranean during that summer, as well as a record dry and hot season [16].

When we compare the two years using FRP (bottom left of figure 6), one can see that there were many fewer areas with higher FRP than those with lower FRP when comparing 2019 to 2018 (148 vs. 160). However, looking at the area where there were the greatest increases in FRP when comparing these years, we find that they were located primarily in the central Aegean region.

In contrast, there was a significant increase in FRP when comparing the two years using FRP (bottom center of figure 6): more than twice as many areas had greater amounts of FRP in 2020 compared to 2019 (193 vs. 157).

Table 2. Summary statistics for cell-level mean FRP and interannual change detection, 2018–2020.

Year	Mean FRP (MW)	Grid cells (n)	Cells increased	Cells decreased
2018	19.0	308	—	—
2019	18.7	317	148	160
2020	23.2	316	193	157

Finally, the difference surface for FRP comparing 2020 to 2018 (bottom right of figure 6) shows that while there were some areas with less FRP in 2020 than in 2018 (172 cells), there were more areas with greater amounts of FRP in 2020 than in 2018 (180 cells), which suggests a positive trend overall in terms of increasing fire activity.

Figure 6. Cell-level mean FRP maps for 2018, 2019, and 2020 (top row), and interannual FRP difference maps (bottom row). Red tones indicate FRP increases; blue tones indicate decreases.

Additionally, the largest clusters of FRP gain when moving westward through Türkiye appear to be located on both sides of the coastal plain extending south-westward from Istanbul and along the western edge of the Central Anatolia Plateau.

4.5 Spatial Clustering of Fire Detections (DBSCAN)

DBSCAN spatial clustering on each year's fire detection data produced 4, 3, and 7 clusters in 2018, 2019, and 2020, respectively. All the fire detections were assigned to one of these clusters in each year. No fire detection was classified as noise, which indicated that the parameters selected (ε=50km; MinPts=5) successfully captured the spatial density distribution of fires occurring in Türkiye. Spatial density distributions were created without artificial fragmentation of the data.

A similar pattern of results occurred in each year with respect to most fire detections being within a single large cluster, and that cluster's centroid is consistently at approximately 37.8 – 38.0 N latitude in the south-central Anatolian region, referred to hereafter as the south-central Anatolian fire belt. This location also represents the area of highest frequency of fire occurrences based upon the KDE and Gi* analyses.

Table 3. DBSCAN clustering results for active fire detections

Year	Clusters (n)	Dominant cluster	Clustered (%)	Centroid lat. (°N)
2018	4	6,889	100	37.9
2019	3	7,392	100	38.0
2020	7	7,745	100	37.8

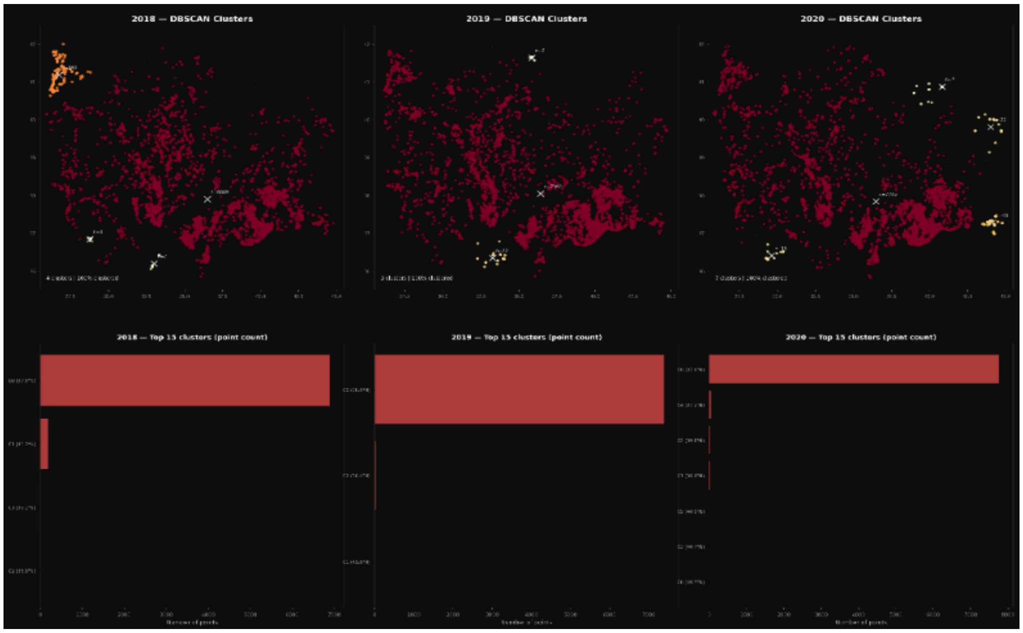

Figure 7. DBSCAN spatial cluster maps (top row) and bar charts of cluster size ranked by point count (bottom row)

As can be seen in Figure 7 (top row), the number of fire detections within this dominant cluster increased over time. Specifically, it went from approximately 6899 detections in 2018 to about 7392 in 2019 and then to just under 7750 detections in 2020. These numbers represent an increase in both the intensity of the clustered fire activity and/or an increase in the amount of space within which that activity was occurring. As such, they indicate that the activity has intensified in this fire belt. In addition to an intensification of activity in the dominant fire belt, there appears to have been a geographic dispersal of activity away from the fire belt. That is, the number of clusters increased from three in 2019 to seven in 2020 (figure 7, bottom row). The new six smaller clusters appear to be located primarily in two regions, the

northeast Anatolian Highlands and eastern Thrace. These are geographic locations where relatively few or no fires had occurred before 2020.

V. DISCUSSION

Analytical results derived from the five methods used in the present study consistently indicate that the fire regime dynamics of Türkiye are characterized by a strong regional dynamic during the 2018–2020 time frame. The coincidence of (a) high FRP-weighted KDE densities, (b) high values for Getis-Ord Gi* z-score, and (c) the centroid of the dominant DBSCAN cluster within the southern Anatolian region, all clearly identify this area as the main fire intensity nucleus in Türkiye. Confidence in identifying this region as a fire intensity nucleus is increased by the fact that these independent measures agree with respect to its location.

A second major result of this analysis concerns the decreasing autocorrelation among fires across the time span covered by the data. Specifically, global Moran's I decreased from an initial value of 0.233 in 2018 to 0.083 in 2020 (a decrease of almost 64%). While a decline in Moran's I can be caused by either reduced overall fire activity or by changes in how fires were distributed in space, there was no evidence of such reductions. For example, total fire activity remained relatively constant as indicated by the increase in mean FRP from 19.0 MW in 2018 to 23.2 MW in 2020; similarly, there was a growth in the number of points in the largest DBSCAN cluster from 6,889 in 2018 to 7,745 in 2020. Therefore, the observed decline in Moran's I indicates that fires had become progressively more dispersed throughout space [28]. In addition, the observation that new DBSCAN clusters appeared in both northeastern Anatolia and eastern Thrace in 2020 also supports this conclusion.

The combination of low DBSCAN cluster numbers (only three clusters) with large amounts of statistically significant Getis-Ord G∗ hotspot values (five cells at HS $\geq$ 95%) from the year 2019 provides an interesting case study for the analytical advantages of both methods. A seeming contradiction can be explained when we consider the scale at which each method is operating. DBSCAN is based upon point detection and will identify areas as one single cluster where points are contiguous and denser than points in other areas. It does not matter how much higher these points are than those around them. On the other hand, Getis-Ord G∗ measures whether or not the FRP value within a cell is significantly higher than the mean across all cells. Thus, in 2019, there were many locations where fires were detected (so very few clusters), yet they were intense enough compared to their surroundings to have statistically significant FRP values (thus, there were a lot of cells with high scores). These interpretations support that the average FRP value for 2019 (18.7 MW) was relatively small on a national basis; however, it was extremely high at certain specific spatial locations [11, 20].

The increased FRP at the national level by 22% from 2018-2020 in conjunction with the increasing spatial distance of fire clusters is indicative of the general trend of increasing fire intensity seen in the Eastern Mediterranean Basin as reported [1] on a larger scale. The high FRP values for 2020 are associated with both documented summer temperature anomalies and precipitation deficit for the years of 2020 within Türkiye, where these contributed to extreme low fuel moistures resulting in extreme fire behavior [28]. Under climate projection scenarios for mid-century [4], it is anticipated that the conditions associated with the fire season of 2020 will be occurring under this type of warming, with much greater frequency throughout the Mediterranean area; indicating that the observed increases in both spatial dispersion and fire intensity could be indicative of a long term shift in fire regimes for Türkiye rather than simply being anomalous.

The FRP difference mapping analysis provides spatially explicit evidence of where fire intensity has increased or decreased at the grid-cell level, offering a directly applicable input for adaptive fire risk zoning. The net change surface (2020−2018) reveals that the most persistent FRP increases are concentrated along the southwestern coastal zone and the Central Anatolian plateau margin precisely the areas where forest cover and fuel loads are highest and where institutional fire suppression capacity may be most stretched during multi-ignition episodes [29]. Integrating iteratively updated FRP difference maps into national fire danger rating systems could enable proactive reallocation of aerial and ground suppression resources ahead of high-risk seasons, a strategy advocated in recent European fire management frameworks [2].

Several limitations of the present analysis should be acknowledged. First, the 0.5° grid resolution, while appropriate for national-scale autocorrelation statistics, cannot resolve sub-grid heterogeneity in FRP or vegetation type, potentially smoothing important local variations in fire behaviour. Second, the MODIS 1 km detection threshold means that small, low-intensity fires which may be ecologically significant in grassland and agricultural contexts are systematically under-represented in the dataset [6]. Furthermore, no land-cover masking was applied prior to the analyses; therefore, the dataset may include agricultural burning events in addition to forest fires. Although this approach is appropriate for characterizing national-scale active fire patterns, future studies could integrate land-cover datasets such as CORINE Land Cover or Copernicus Land Monitoring Service to distinguish forest fires from agricultural burning and other fire types. Third, the three-year study period, while sufficient for interannual comparison, is too short to distinguish multi-year climate forcing from decadal-scale fire regime trends; a longer time series would be required to confirm the dispersal signal identified here. Finally, the absence of coincident meteorological and fuel moisture data precludes direct attribution of observed spatial patterns to specific climatic drivers, a limitation that could be addressed in future work through integration with ERA5 reanalysis or MODIS land surface temperature products [28].

VI. CONCLUSIONS

This study applied an integrated five-step spatial analysis pipeline comprising FRP-weighted kernel density estimation, global Moran's *I*, Getis-Ord *Gi** hotspot analysis, FRP difference mapping, and DBSCAN clustering to MODIS Collection 6.1 active fire observations across Türkiye for the period 2018–2020. Results have consistently identified the south central Anatolia region (37°–38°N) as the principal focal point of high-intensity fires throughout Türkiye, due to both high levels of FRP weighted density during the study period and the statistical significance of localized hotspots in 2019; additionally, it has been found that the centroid of the most intense DBSCAN cluster is located within this region. Additionally, at a national level, mean FRP increased by nearly 22% from 2018 (19.0 MW) to 2020 (23.2 MW); and the global autocorrelation index decreased by approximately 64%. Thus, these findings suggest that there is an increase in overall fire intensity, with a corresponding increase in the geographic area burned.

Methodologically, this research demonstrates how combining multiple types of spatial analyses, such as global autocorrelation measures (e.g., Moran's I), localized hotspot identification techniques, and density-based clustering, can provide much greater detail on how fire regimes are organized spatially than could be provided using any one technique alone. The complementarities of Moran's I and DBSCAN were demonstrated in the analysis of 2019, when each method independently detected different, yet consistent, components of what would appear to be the same general spatial organization. The reproducible Python code used in this project also establishes a transferable methodology for analysing MODIS fire data in similar regions of the Mediterranean or in areas prone to wildfires [24, 26].

The conclusions from the results have important operational implications for the development of fire risk management strategies in Türkiye. The stable position of the South-Central Anatolia Fire Belt throughout all three years provides support for the investment of permanent early warning/detection systems in this region. The emergence of additional DBSCAN clusters in Northeastern Anatolia and Eastern Thrace in 2020 indicates that zoning frameworks for fire risks need to be reviewed at least annually to account for shifts in high-risk zones due to changing climatic conditions and vegetation dryness [5]. The FRP difference maps developed using the methodology presented in this article provide a direct, satellite-based method for identifying locations experiencing increased fire intensity. This provides a means to develop evidence-based priorities for prescribed burns, vegetation management, and community preparation programs [30, 32].

Future studies could extend the time frame for the temporal coverage of this study to include the devastating 2021 and subsequent fire seasons, thus providing a basis to determine if the observed trends of dispersion and increasing intensity were sustained or reversed after the study period. In addition, integration of MODIS FRP data with the ERA-5 fire weather indexes, MODIS land surface temperatures, and NDVI/EVI vegetation health indicators will provide the capability to directly relate spatial fire occurrences to specific meteorological and/or fuel state factors.

REFERENCES

[1] Jones, M. W., Abatzoglou, J. T., Veraverbeke, S., Andela, N., Lasslop, G., Forkel, M., Smith, A. J. P., Burton, C., Betts, R. A., van der Werf, G. R., Sitch, S., Canadell, J. G., Santín, C., Kolden, C., Doerr, S. H., & Le Quéré, C. (2022). Global and regional trends and drivers of fire under climate change. Reviews of Geophysics, 60(3), e2020RG000726. https://doi.org/10.1029/2020RG000726

[2] Bowman, D. M. J. S., Williamson, G. J., Abatzoglou, J. T., Kolden, C. A., Cochrane, M. A., & Smith, A. M. S. (2020). Human exposure and sensitivity to globally extreme wildfire events. Nature Ecology & Evolution, 1, 58–64. https://doi.org/10.1038/s41559-016-0058

[3] Lionello, P., & Scarascia, L. (2018). The relation between climate change in the Mediterranean region and global warming. Regional Environmental Change, 18(5), 1481–1493. https://doi.org/10.1007/s10113-018-1290-1

[4] Ruffault, J., Curt, T., Moron, V., Trigo, R. M., Mouillot, F., Koutsias, N., Pimont, F., Martin-StPaul, N., Barbero, R., Dupuy, J.-L., Russo, A., & Belhadj-Khedher, C. (2020). Increased likelihood of heat-induced large wildfires in the Mediterranean Basin. Scientific Reports, 10, 13790. https://doi.org/10.1038/s41598-020-70069-z

[5] Karali, A., Hatzaki, M., Giannakopoulos, C., Roussos, A., Xanthopoulos, G., & Tenentes, V. (2021). Sensitivity and evaluation of current fire risk and future projections due to climate change: The case study of Greece. Natural Hazards and Earth System Sciences, 14(1), 143–153. https://doi.org/10.5194/nhess-14-143-2014

[6] Giglio, L., Schroeder, W., & Justice, C. O. (2016). The collection 6 MODIS active fire detection algorithm and fire products. Remote Sensing of Environment, 178, 31–41. https://doi.org/10.1016/j.rse.2016.02.054

[7] Wooster, M. J., Roberts, G., Perry, G. L. W., & Kaufman, Y. J. (2005). Retrieval of biomass combustion rates and totals from fire radiative power observations: FRP derivation and calibration relationships between biomass consumption and fire radiative energy release. Journal of Geophysical Research: Atmospheres, 110(D24). https://doi.org/10.1029/2005JD006318

[8] Kaiser, J. W., Heil, A., Andreae, M. O., Benedetti, A., Chubarova, N., Jones, L., Morcrette, J.-J., Razinger, M., Schultz, M. G., Suttie, M., & van der Werf, G. R. (2012). Biomass burning emissions estimated with a global fire assimilation system based on observed fire radiative power. Biogeosciences, 9(1), 527–554. https://doi.org/10.5194/bg-9-527-2012

[9] Bowman, A. W., & Azzalini, A. (1997). Applied smoothing techniques for data analysis. Oxford University Press.

[10] Moran, P. A. P. (1950). Notes on continuous stochastic phenomena. Biometrika, 37(1–2), 17–23. https://doi.org/10.2307/2332142

[11] Anselin, L., Syabri, I., & Kho, Y. (2006). GeoDa: An introduction to spatial data analysis. Geographical Analysis, 38(1), 5–22. https://doi.org/10.1111/j.0016-7363.2005.00671.x

[12] Getis, A., & Ord, J. K. (1992). The analysis of spatial association by use of distance statistics. Geographical Analysis, 24(3), 189–206. https://doi.org/10.1111/j.1538-4632.1992.tb00261.x

[13] Ester, M., Kriegel, H.-P., Sander, J., & Xu, X. (1996). A density-based algorithm for discovering clusters in large spatial databases with noise. Proceedings of the 2nd International Conference on Knowledge Discovery and Data Mining (KDD-96), 226–231.

[14] Rodrigues, M., Jiménez-Ruano, A., Peña-Angulo, D., & de la Riva, J. (2018). A comprehensive spatial–temporal analysis of driving factors of human-caused wildfires in Spain using Geographically Weighted Logistic Regression. Journal of Environmental

Management, 225, 177–192. https://doi.org/10.1016/j.jenvman.2018.07.098

[15] Türkes, M. (2012). Türkiye'de gözlenen ve öngörülen iklim değişikliği, kuraklık ve çölleşme. Ankara Üniversitesi Çevrebilimleri Dergisi, 4(2), 1-32.

[16] Turco, M., Rosa-Cánovas, J. J., de Bono, A., Jerez, S., Doblas-Reyes, F. J., Christensen, O. B., & Moreno, J. M. (2018). Exacerbated fires in Mediterranean Europe due to anthropogenic warming projected with non-stationary climate-fire models. Nature Communications, 9(1), 3821. https://doi.org/10.1038/s41467-018-06358-z

[17] Anselin, L. (2022). Spatial econometrics. Handbook of spatial analysis in the social sciences, 101-122.

[18] Renshaw, E., Cliff, A. D., & Ord, J. K. (1982). Spatial processes, models and applications. Biometrics, 38(1), 287.

[19] Bivand, R. S., Pebesma, E., & Gómez-Rubio, V. (2013). Applied spatial data analysis with R (2nd ed.). Springer. https://doi.org/10.1007/978-1-4614-7618-4

[20] Mitchell, A. (2005). The ESRI guide to GIS analysis, Volume 2: Spatial measurements and statistics. ESRI Press.

[21] Singh, A. (1989). Review article: Digital change detection techniques using remotely-sensed data. International Journal of Remote Sensing, 10(6), 989–1003. https://doi.org/10.1080/01431168908903939

[22] Sinnott, R. W. (1984). Virtues of the Haversine. Sky and Telescope, 68(2), 159.

[23] Schubert, E., Sander, J., Ester, M., Kriegel, H.-P., & Xu, X. (2017). DBSCAN revisited, revisited: Why and how you should (still) use DBSCAN. ACM Transactions on Database Systems, 42(3), 1–21. https://doi.org/10.1145/3068335

[24] Rey, S. J., & Anselin, L. (2010). PySAL: A Python library of spatial analytical methods. In M. M. Fischer & A. Getis (Eds.), Handbook of applied spatial analysis (pp. 175–193). Springer. https://doi.org/10.1007/978-3-642-03647-7_11

[25] Virtanen, P., Gommers, R., Oliphant, T. E., Haberland, M., Reddy, T., Cournapeau, D., Burovski, E., Peterson, P., Weckesser, W., Bright, J., van der Walt, S. J., Brett, M., Wilson, J., Millman, K. J., Mayorov, N., Nelson, A. R. J., Jones, E., Kern, R., Larson, E., & SciPy 1.0 Contributors. (2020). SciPy 1.0: Fundamental algorithms for scientific computing in Python. Nature Methods, 17, 261–272. https://doi.org/10.1038/s41592-019-0686-2

[26] Pedregosa, F., Varoquaux, G., Gramfort, A., Michel, V., Thirion, B., Grisel, O., Blondel, M., Prettenhofer, P., Weiss, R., Dubourg, V., Vanderplas, J., Passos, A., Cournapeau, D., Brucher, M., Perrot, M., & Duchesnay, E. (2011). Scikit-learn: Machine learning in Python. Journal of Machine Learning Research, 12, 2825–2830.

[27] Hunter, J. D. (2007). Matplotlib: A 2D graphics environment. Computing in Science & Engineering, 9(3), 90–95. https://doi.org/10.1109/MCSE.2007.55

[28] Abatzoglou, J. T., Williams, A. P., & Barbero, R. (2019). Global emergence of anthropogenic climate change in fire weather indices. Geophysical Research Letters, 46(1), 326–336. https://doi.org/10.1029/2018GL080959

[29] San-Miguel-Ayanz, J., Moreno, J. M., & Camia, A. (2013). Analysis of large fires in European Mediterranean landscapes: Lessons learned and perspectives. Forest Ecology and Management, 294, 11–22. https://doi.org/10.1016/j.foreco.2012.10.050

[30] Behnisch, M., Krüger, T., & Jaeger, J. A. (2022). Rapid rise in urban sprawl: Global hotspots and trends since 1990. PLOS Sustainability and Transformation, 1(11), e0000034.

[31] Jordahl, K., Van den Bossche, J., Fleischmann, M., Wasserman, J., McBride, J., Gerard, J., Tratner, J., Perry, M., Badaracco, A. G., Farmer, C., Hjelle, G. A., Snow, A. D., Cochran, M., Gillies, S., Culbertson, L., Teigen, M., Hayden, A., & Filipe, E. A. I. (2021). geopandas/geopandas: v0.9.0. Zenodo. https://doi.org/10.5281/zenodo.4569086

[32] Sá, A. C. L., Pereira, J. M. C., Charlton, M. E., Mota, B., Barbosa, P. M., & Stewart Fotheringham, A. (2017). The pyrogeography of sub-Saharan Africa: A study of the spatial non-stationarity of fire–environment relationships using GWR. Journal of Geographical Systems, 13(3), 227–248. https://doi.org/10.1007/s10109-010-0123-7